Nonlinear Dynamics **25:** 111–132, 2001.
© 2001 *Kluwer Academic Publishers. Printed in the Netherlands.*

Spatially Localized Models of Extended Systems

RALF W. WITTENBERG*
Institute for Mathematics and its Applications, University of Minnesota, 400 Lind Hall, 207 Church Street SE, Minneapolis, MN 55455, U.S.A.

PHILIP HOLMES
Program in Applied and Computational Mathematics, Princeton University, Fine Hall, Washington Road, Princeton, NJ 08544, U.S.A.

(Received: 18 February 1999; accepted: 31 August 1999)

Abstract. We investigate the construction of low-dimensional spatially localized models of extended systems. Specifically, the Kuramoto–Sivashinsky (KS) equation on large one-dimensional domains displays spatiotemporally complex dynamics that are remarkably well-localized in both real and Fourier space, as demonstrated by a (spline) wavelet representation. We show how wavelet projections may be used to construct various localized, relatively low-dimensional models of KS spatiotemporal chaos. There is persuasive evidence that short, periodized systems, internally forced at their largest scales, form minimal models for chaotic dynamics in arbitrarily large domains. Such models assist in the understanding of extended systems.

Keywords: Spatiotemporal chaos, low-dimensional models, wavelets, Kuramoto–Sivashinsky equation.

1. Introduction

For the prediction, simulation, control and understanding of high-dimensional systems with complex spatiotemporal dynamics, one frequently seeks low-dimensional models capturing the essential features. One approach toward obtaining such models is to propose, on the basis of considerations such as relevant symmetries and physical principles, relatively 'simple' *a priori* governing equations to model the system. Alternatively, one can project known governing equations onto the 'relevant' modes, obtained for instance through the proper orthogonal decomposition (POD), via Galerkin projection. Crucial aspects of this procedure are that the most essential modes are isolated and retained, and that the effects of neglected modes are modeled appropriately. The goal is to obtain a, hopefully tractable, system of the form

$$\dot{\mathbf{a}} = \mathbf{f}(\mathbf{a}, \mathbf{b}) \tag{1}$$

for the retained 'internal' modes of the model $\mathbf{a}$, where in the present procedure, the excluded, or neglected modes $\mathbf{b}$ are externally specified, rather than being 'slaved' to the internal modes. That is, while the internal modes $\mathbf{a}$ are analogous to the span of a 'critical' eigenspace, the modes $\mathbf{b}$ will not be represented in the form $\mathbf{b}(\mathbf{a})$, as in a center, center-unstable or inertial manifold reduction, since they derive from dynamics that are largely supported outside the model domain, or that involve length scales exceeding those of the model.

The latter approach has been successfully implemented and extensively studied in the last decade or so, particularly in the context of fluids [1, 10]. One identifies coherent structures

* Current address: Department of Mathematics, University of Michigan, 2072 East Hall, 525 East University Avenue, Ann Arbor, MI 48109, U.S.A. (E-mail: ralf@math.lsa.umich.edu).

via the POD (or Karhunen–Loève decomposition), performs a Galerkin projection of the governing Navier–Stokes equations onto the most energetic modes, and models the neglected modes to obtain a closed model capturing the essential dynamics.

In this paper, we investigate the construction of low-dimensional spatially localized models to understand spatiotemporally complex dynamics in a particular system. Our approach, while motivated by and related to the above-mentioned fluid studies, is novel and involves the use of wavelets for the study of PDEs and extended dynamical systems, exploiting them to extract localized models in space and scale. Our model problem is the one-dimensional Kuramoto–Sivashinsky (KS) equation,

$$u_t + u_{xxxx} + u_{xx} + uu_x = 0, \quad x \in [0, L], \tag{2}$$

where $u_t = \partial u/\partial t$, $u_x = \partial u/\partial x$, and after rescaling the only control parameter is the system length L; we assume periodic boundary conditions and set the (conserved) spatial mean to zero. For future reference, we rewrite the KS equation in the symbolic form

$$u_t = \mathcal{L}u + u\mathcal{D}u, \tag{3}$$

where $\mathcal{L} = -\partial_x^4 - \partial_x^2$, and $\mathcal{D} = -\partial_x$. For remarks on the derivation and applications of the KS equation, see, for instance, [22].

In (2), the u_{xx} term is responsible for energy production, destabilizing large scales, while the u_{xxxx} term strongly damps small scales, and the uu_x term stabilizes by nonlinear coupling, transferring energy between large and small scales. From the evolution equation for the Fourier modes $\hat{u}_q$ (where the Fourier representation is defined by $u(x, t) = \sum_q \hat{u}_q(t) \exp(\mathrm{i}qx)$, $q = 2\pi n/L$, $n \in \mathbb{Z}$), it is readily apparent that the number of linearly unstable Fourier modes is proportional to the system length L. The effect of nonlinear coupling between excited and damped modes is to yield complicated dynamics, with an intricate bifurcation sequence as L increases, and for large enough L, extensive 'spatiotemporal chaos' (STC) with a positive density of positive Lyapunov exponents. Consequently, this system is popularly studied as a prototype of complex spatiotemporal dynamics in a partial differential equation (PDE), as visualization of the solutions of this equation in the STC regime (see Figure 1) suggests the presence of structures having characteristic space and time scales, and localized 'events' resembling short-L solutions. This motivates the search for localized models to represent the evolution and interactions of the coherent structures.

Due to the periodic boundary conditions, the POD approach [10] does not yield localized modes, as the POD eigenmodes for such a translationally invariant system are Fourier modes. This observation led to the proposal of localization via wavelet-based models [3, 6]. In previous work [22], we showed how a projection onto wavelet modes captured the space and scale localization of the dynamics remarkably well, and we obtained a characterization of the dynamics in terms of these modes. In the present paper, after reviewing those results in Section 2, we show how wavelets permit the extraction of relatively low-dimensional local models which capture the essentials of the complex dynamics. We emphasize that in contrast to the usual POD paradigm for extracting coherent structures, the wavelet modes are not intended to reproduce the typical shapes of the structures; rather, we use them to isolate features that are localized in both physical and Fourier space. This notion differs from that of spatially localized modes (Anderson localization) discussed in other papers in this issue: for us wavelets provide 'windowing' tools to examine local properties of solutions which are statistically homogeneous and spatially distributed.

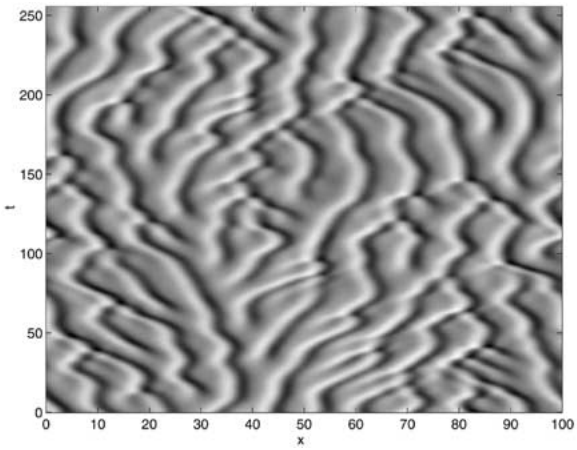

Figure 1. Gray-scale representation of the evolution of a solution of the KS equation (2) on the spatiotemporally chaotic attractor, showing typical local 'events', the interactions of coherent structures at a characteristic scale. Lighter shading indicates local maxima, darker shows minima, and the shading interpolates between extreme values of white at $u = +3.5$ and black at $u = -3.5$.

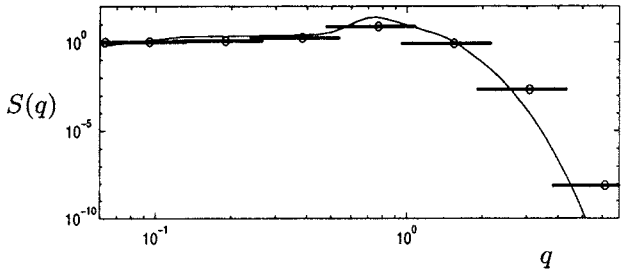

Figure 2. Power spectrum $S(q)$, compared to the energy per individual wavelet at each level j (horizontal lines). The wavelet distribution is plotted with the center and range of 99% of the support in Fourier space. From [22].

2. Characterization of Spatiotemporally Chaotic KS Dynamics

Spatiotemporal chaos (STC) in the KS equation has been extensively characterized and reported in the literature; see, for instance, [11, 17, 22], and the review in [20] (particularly chapters 1 and 4), which contains many additional details and references. Of particular importance in understanding the qualitative dynamics in the extensively chaotic regime is the power spectrum $S(q)$, or mean energy per Fourier mode, shown in Figure 2 [16, 19]. Here the power spectrum is defined in terms of the Fourier modes $\hat{u}_q$ by $S(q) = L\langle \hat{u}_{-q}\hat{u}_q \rangle$, and by invoking ergodicity, we replace ensemble averages $\langle\cdot\rangle$ on the attractor by time averages along a single solution trajectory.

The shape of the power spectrum reveals three characteristic regimes of the overall dynamics at different scales. The spectrum is almost flat in the *large* scale (low-q) region, reminiscent of a thermodynamically equilibrated regime with equipartition of energy. The *active* scales contain most of the energy, and have a pronounced peak for $q = q_m$ near the most linearly unstable mode, $q_m \approx q_0 = 1/\sqrt{2}$; that is, the local interactions occur at length scales near $l_m = 2\pi/q_m \approx 2\pi\sqrt{2}$. There is exponential decay of energy due to strong dissipation at the *small* scales.

2.1. The Wavelet Decomposition

Fourier-based properties such as the power spectrum are continuous in q, giving no separation of scales; we may wish to group ranges of Fourier modes to separate and distinguish between characteristic features of the dynamics at different scales. Furthermore, the Fourier representation is unable to capture any properties that arise from spatial localization, as each Fourier basis function is uniformly supported on the entire domain. This motivates the use of a basis localized in space and scale to detect dynamic features largely due to concentrated events at characteristic length scales, and wavelets are well suited to this purpose [22]. Following [3, 6, 7] we use a set of functions $\{\psi_{jk}\}$, symmetric about their centers $x_{jk} = L2^{-j}(k + 1/2)$, indexed by the scale, or wavelet *level*, j, with k denoting the horizontal position within the level (by our choice of convention, $j = 0$ refers to the largest, or coarsest, scale, while increasing j implies 'zooming in' to smaller, or finer, scales). It is frequently convenient to visualize the set of wavelets in terms of a 'wavelet pyramid', with rows arranged in decreasing order of scale (increasing j), and horizontal location within each row representing the central position x_{jk}, as in the schematic cartoons of Figures 4, 5 and 8.

These wavelet functions $\{\psi_{jk}\}$ form an orthonormal basis for zero mean, finite energy periodic functions on $[0, L]$ of periodized, m-th order spline wavelets [15], which are of class C^{m-2}, have $m - 1$ vanishing moments, exponential decay in x, and algebraic decay in q as $|q| \to 0$ and $|q| \to \infty$. In terms of this basis, in the following we use the wavelet representation of the solution $u(x, t)$ of the KS equation:

$$u(x,t) = \sum_{j=0}^{J} \sum_{k=0}^{2^j-1} a_{jk}(t)\psi_{jk}(x) = \sum_{\alpha} a_\alpha(t)\psi_\alpha(x). \tag{4}$$

The KS equation in terms of the wavelet coefficients, obtained by Galerkin projection of the governing equation (2) onto the decomposition (4), is then given by

$$\frac{\mathrm{d}}{\mathrm{d}t}a_\alpha(t) = \sum_{\alpha'} l_{\alpha\alpha'}a_{\alpha'} + \sum_{\alpha',\alpha''} n_{\alpha\alpha'\alpha''}a_{\alpha'}a_{\alpha''}, \tag{5}$$

where

$$l_{\alpha\alpha'} = -\int_0^L \psi_\alpha \left(\partial_{xx}\psi_{\alpha'} + \partial_{xxxx}\psi_{\alpha'}\right) \mathrm{d}x, \quad n_{\alpha\alpha'\alpha''} = -\int_0^L \psi_\alpha\psi_{\alpha'}\partial_x\psi_{\alpha''}\,\mathrm{d}x,$$

and α represents the multi-index (j, k). The time-dependent wavelet coefficients $a_{jk}(t) = a_\alpha(t)$ satisfying (5) reveal the behavior of $u(x, t)$ at scale or level j and position given by k.

The results in this paper on wavelet characterization and models for the KS equation are all reported for $L = 100$, well within the STC regime. For other lengths, the results are qualitatively similar, but the details depend on the interplay between wavelet and intrinsic length scales, specifically, on the relation between the distance $l_j = L2^{-j}$ between adjacent wavelets at level j of the dyadic wavelet decomposition and the characteristic length of the dynamics l_m [20]. For $L = 100$, the peak of the energy spectrum is located in wavelet level $j = 4$, as seen in Figure 2, which shows the energy per individual wavelet by comparison with the Fourier power spectrum, and confirms that wavelets are well-localized in Fourier space. On combining the energy distribution per wavelet with the number 2^j of wavelets at

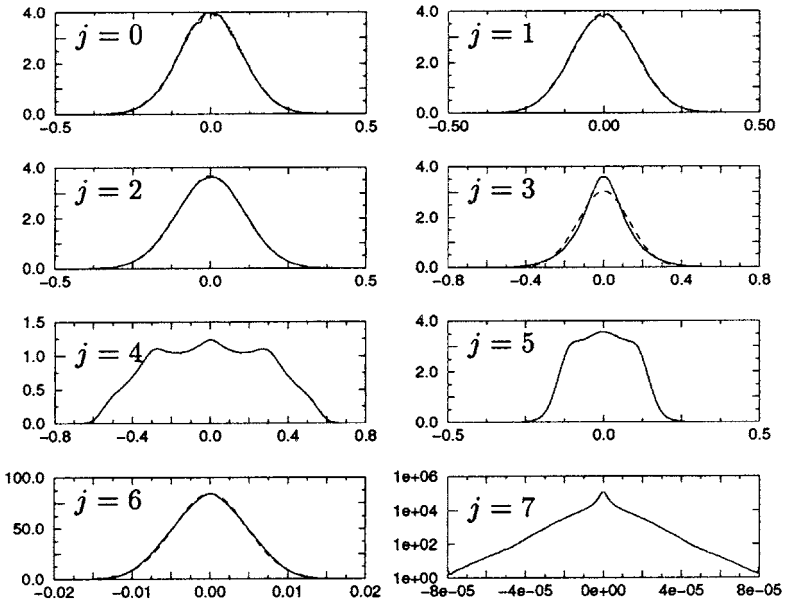

Figure 3. Probability density functions for the wavelet coefficients at each level $j = 0, \ldots, 7$, for $L = 100$. For $j = 0$-3 and 6, a best-fit Gaussian distribution is superposed (dashed line); the logarithmic axis for $j = 7$ indicates a near-exponential distribution. The figure for $j = 0$ also contains the PDF (dotted line) for a long-time simulation of the stochastic model (7), which is nearly coincident with the PDF from the KS simulation.

level j, the fraction of energy per wavelet level may be computed, and allows us to clearly distinguish between the levels with distinct behaviors. In fact, the active, energetic scales, levels $j = 3$, 4 and 5, together account for over 95% of the total energy, with level 4 alone containing about 71%. The large scales, levels 0, 1 and 2, contain under 5% of the total energy, and the small scale levels $j = 6, 7, \ldots$ are strongly damped with less than 0.1% of the energy. Inspection of time series and temporal correlations at the different levels indicates slow large-scale dynamics, correlation times of the order of $\tau \approx 10$ for the active scales – comparable to those of the system as a whole, and more rapid and intermittent behavior at the small scales.

2.2. Probability Distributions of Wavelet Coefficients

The most striking distinctions between the different scales and their dynamical significance are displayed in Figure 3 by the probability distribution functions (PDFs) for different j, which clearly show how the wavelet representation captures both scale and spatially localized information. At large scales, the distributions are Gaussian, and the dynamics resemble slow noise. This is consistent with the conjecture [23] that the large-scale dynamics may be described by a noise-driven Burgers equation with a positive effective viscosity $\nu > 0$,

$$u_t = \nu u_{xx} + \lambda u u_x + f, \tag{6}$$

where the stochastic forcing term may be interpreted as the derivative of Gaussian white noise. In this picture, the (deterministically chaotic) active and small scales simulate the effect of a random forcing on the large scales, as well as renormalizing the viscosity through nonlinear coupling. The form of this effective equation is motivated by symmetry principles, and the asymptotic validity of this description has been confirmed by several analytical and numerical

studies [13, 18]; see [20, sec. 4.2.2]. The equation (6) has generated much interest since it was shown [12] that its integral form, known as the KPZ equation, is the simplest equation describing the kinetic roughening of growing interfaces with stochastic local dynamics [2, 8].

For modeling purposes, one can exploit the observed Gaussian dynamics of Figure 3 by replacing the 'noisy' large scales with an autonomously generated stochastic process motivated by the effective description (6). Computations [9, 18] of the parameters in (6) relevant to the KS equation show that for lengths L less than several thousand, the $\lambda u u_x$ term is asymptotically irrelevant to the scaling of solutions; so for the lengths we are interested in, we may linearize (6) by setting $\lambda = 0$. Additionally, the forcing term f has finite correlation time τ_f of order 10 [24], as expected since it is derived from the deterministic active and small scales. This suggests a linear stochastic model in which we use (6) with $\lambda = 0$ in Fourier space, and model the forcing with the simplest Langevin equation form that gives finite-time (exponential) correlations in the long-time limit. Our stochastic description for a large-scale Fourier mode $\hat{v}_q$ driven by colored noise is thus

$$\frac{\mathrm{d}}{\mathrm{d}t}\hat{v}_q = -\nu q^2\ \hat{v}_q + \hat{f}_q, \qquad \frac{\mathrm{d}}{\mathrm{d}t}\hat{f}_q = -\frac{1}{\tau_f}\ \hat{f}_q + \sqrt{D_f}\ \hat{\eta}_q, \tag{7}$$

where $D_f = Dq^2/L\tau_f^2$, and $\hat{\eta}_q$ is zero-mean, unit-variance, Gaussian white noise, with covariance $\langle \hat{\eta}_q(t)\hat{\eta}_{q'}(t')\rangle = \delta_{q+q',0}\delta(t-t')$. An advantage of this description is that the parameters in the effective forced Burgers description have all been determined for the KS equation, so no fitting is required; we use the values $D = 17.9$, $\nu = 7.5$ and $\tau_f = 7.0$ quoted in [9].

In the limit of long times and large scales ($q \to 0$), the spectra and correlations for this modified Ornstein-Uhlenbeck process (Langevin equation with colored noise) agree with theoretical predictions for the forced Burgers/KPZ model (6). With the values for D, ν and τ_f given above, we have simulated our stochastic model (7), and found it to reproduce the large-scale KS behavior extremely well, as shown in the PDF for level $j = 0$ in Figure 3 (our model is also appropriate for large-scale wavelets, since these are superpositions of few Fourier modes). We shall use the model (7) in numerical experiments below.

At the energetic scales $j = 3$, 4 and 5, the wavelet coefficient PDFs are strikingly different from any observed in the Fourier representation. The $j = 3$ level shows a distinct steepening of the distribution relative to a Gaussian, while levels $j = 4$ and (to a slightly lesser extent) $j = 5$ show strongly nonequilibrium PDFs, comparable to the distributions for pointwise values of u [9]: a broad, triple-humped distribution, superposing a peak at 0 and a double-humped peak reminiscent of cellular (sinusoidal-like) solutions. At these scales, the support of the wavelets is comparable to the characteristic intrinsic wavelength l_m of the dynamics, and the wavelet coefficients appear to capture on average the spatially local structures and events at the active scales.

The PDF for level $j = 6$ is again almost Gaussian; it is interesting that such an equilibrium distribution should appear well within the dissipative range, and this property is incompletely understood. At the smallest scales, $j \geq 7$, the effects of strong dissipation are apparent, and the wavelet coefficients display near-exponential PDFs reminiscent of those associated with small-scale intermittency in turbulence: the small-scale coefficients remain near zero most of the time, and undergo occasional excursions of relatively large amplitude driven by events at larger scales, and associated with the passage of 'coherent structures', that is, peaks or troughs of the field u.

2.3. Space Localization

Visual inspection of the collision and birth of peaks prevalent throughout the STC regime, as in Figure 1, suggests that the interactions of coherent structures are spatially localized [22]. Computation of characteristic lengths, such as those associated with the exponential decay of the two-point correlation function or the mutual information, confirms that sufficiently distant spatial locations are statistically independent; comparison of the bulk KS dynamics in the presence of changing boundary conditions also indicates the absence of significant interactions beyond a certain distance.

In [22] we presented an alternative, stronger view of spatial localization, showing with the aid of the wavelet Galerkin form of the KS equation (5) that $\bar{l}_c \approx 25$ is a good estimate of an dynamical interaction distance, capturing the localization of *instantaneous* coupling between modes instead merely of statistical averages on the attractor. Specifically, we observed that the Galerkin coefficients $l_{\alpha\alpha'}$ in (5) describe the coupling between wavelets ψ_α and $\psi_{\alpha'}$ separated by a distance $d_{\alpha\alpha'} = |x_\alpha - x_{\alpha'}|$, and decay due to the spatial exponential decay of $\psi(x)$; similarly for $n_{\alpha\alpha'\alpha''}$. This allows us to manipulate the dynamics, eliminating all coupling beyond an interaction distance l_c by setting $l_{\alpha\alpha'} = 0$ when $d_{\alpha\alpha'} > l_c$, and similarly for the nonlinear term. A range of experiments with varying l_c showed that for large enough l_c, we recover the essential KS dynamics, while decreasing l_c, cutting more and more interactions, significantly alters the dynamics, causing departures from typical events, space and time scales, inducing shifts in the energy distributions to larger scales, and frequent divergence and blowup of the temporal evolution due to disruption of the energy dissipation mechanisms. This led us to estimate a typical *dynamical* interaction length $\bar{l}_c \approx 25$, beyond which cutting interactions significantly disrupts the KS dynamics, and suggested that in low-dimensional 'short' models for the observed spatiotemporally complex behavior as described in Section 3 below, wavelets should be coupled, either to other modes or to external forcing, up to at least a distance $\sim \bar{l}_c$, to ensure sufficient interactions.

2.4. Scale-by-Scale Structure of the Dynamics

Whereas the above statistical results indicate how wavelet spectra and PDFs can discriminate between *averaged* contributions of different scales, we may also use wavelets as an experimental tool to discern the detailed *dynamical* significance of different wavelet levels to the overall spatiotemporally complex dynamics; the ensuing insights will form a further ingredient for our construction of local models.

In principle, our experiments here and in Section 3 focus on the evolution of a set of internal modes of our model, $\{a_\alpha\}$, $\alpha \in \mathbf{B}$, where $\mathbf{B}$ is a subset of the complete set $\mathbf{A}$ of wavelet indices; for the experiments of this section, $\mathbf{B}$ contains complete wavelet levels, whereas the models of Section 3 use a spatially localized subset, or 'box', of wavelet modes. These internal modes are forced by the external modes $\{b_{\alpha'}\}$, $\alpha' \notin \mathbf{B}$, so that the a_α satisfy

$$\frac{\mathrm{d}}{\mathrm{d}t}a_\alpha = \sum_{\alpha' \in \mathbf{B}} l_{\alpha\alpha'} a_{\alpha'} + \sum_{\alpha' \notin \mathbf{B}} l_{\alpha\alpha'} b_{\alpha'} + \sum_{\alpha', \alpha'' \in \mathbf{B}} n_{\alpha\alpha'\alpha''} a_{\alpha'} a_{\alpha''} + \sum_{\alpha' \in \mathbf{B},\ \alpha'' \notin \mathbf{B}} (n_{\alpha\alpha'\alpha''} + n_{\alpha\alpha''\alpha'}) a_{\alpha'} b_{\alpha''} + \sum_{\alpha', \alpha'' \notin \mathbf{B}} n_{\alpha\alpha'\alpha''} b_{\alpha'} b_{\alpha''}, \quad \alpha \in \mathbf{B}. \tag{8}$$

In practice, this formulation is equivalent to overwriting modal coefficients at each time step, and this is the method we use for our experiments. Specifically, we integrate the full

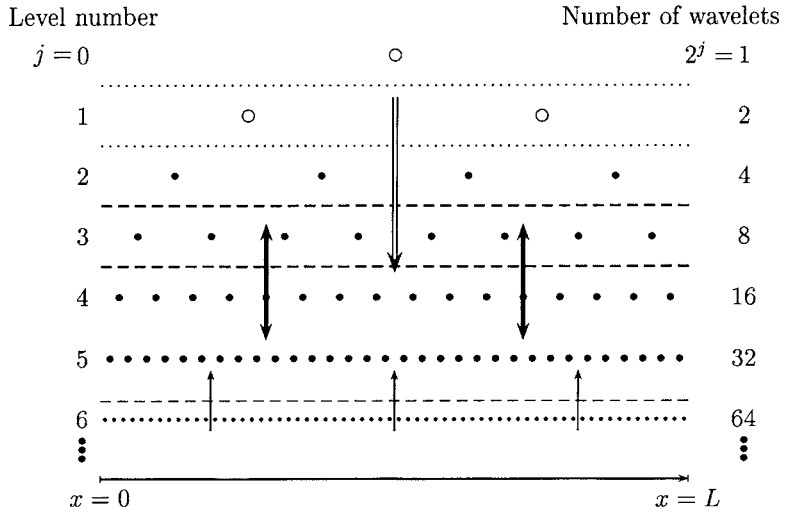

Figure 4. Schematic representation of Section 2.4, in which the interactions of complete wavelet levels and their contributions to the overall dynamics are investigated, particularly the influence of large scales on the active scale modes.

KS equation for the wavelet modes $\{a_\alpha\} = \{a_{jk}\}$ using a wavelet pseudospectral solver. We can then, say, eliminate wavelet level j by setting all the modes $b_{jk'}$ at that level to zero after each time step; alternatively, we can force at particular modes by replacing them with values computed from independent KS integrations, in which case the $\{b_{\alpha'}\}$ satisfy (5), or via an autonomous model of some kind for the $\{b_{\alpha'}\}$ (see [4] for a similar approach to the investigation of two-dimensional Navier–Stokes dynamics). By successively eliminating or driving different levels or combinations of levels, we deduce their respective contributions to the spatiotemporally chaotic dynamics, as suggested in the cartoon of Figure 4; in Section 3 we use a similar approach to driving a local set of modes to evaluate various localized models.

From the results of numerous such experiments for $L = 100$, described in [22] and more fully in [20], we find that the smallest scales, $j \geq 6$, are essentially irrelevant to the dynamics, being slaved to the larger scales, and may be eliminated at little cost except to detailed tracking. The most active, energetic scales $j = 4$ and 5 are crucial for both the characteristic spatial structure and the energy transfer mechanism, and must be included as internal modes in any model. Experiments in which some or all of the large-scale levels $j = 0$–2 are 'turned off', demonstrate that these scales contribute the noisy excitation that prevents the system from settling down in a cellular state and maintains the spatiotemporal disorder, though no one of these levels itself is vital to this purpose. Indeed, the large scales can drive the active scales even in the absence of intermediate levels, indicating that nonlocal energy transfer occurs. Level $j = 3$, intermediate between the large and most active scales, appears to play a major role in sustaining the typical 'events', the interactions of coherent structures through the creation and annihilation of defects.

In an autonomous model for a well-chosen subset of the total set of modes of the KS equation, we shall need to model neglected modes with external forcing terms. It is important to know how much freedom we have in this choice: how faithful does the forcing need to be to the 'true' behavior to induce qualitatively and, if possible, quantitatively correct dynamics? Answers to this question yield much information on the essential ingredients of the complex

dynamics, and the robustness of the STC state. In view of spatial translational invariance and the strong scale-dependence of the behavior of the wavelet modes, as before we investigate the effects of forcing on a scale-by-scale basis [20, ch. 5].

As we observed from eliminating individual levels, forcing at levels $j \geq 6$ has negligible effect on the large- and active-scale dynamics, there being little back-propagation of energy; consequently, these small-scale levels will typically be neglected in the models of Section 3. In contrast, driving at or manipulating the most energetic levels $j = 4$ and/or 5, even with correct statistics obtained from an independent integration of the KS equation, sufficiently destroys the essential phase relationships and energy transfer mechanisms to lead to finite-time blowup. At the large-scale levels there is more flexibility, and driving them from an independent KS run certainly yields the 'correct' dynamics and statistics. In fact, we may go further: We have already observed in Section 2.2 that the statistics at the large scales are Gaussian, and may be well-simulated by an autonomously generated linear stochastic process. However, the KS equation is completely deterministic, and we might conceivably expect its characteristic dynamics to depend on correlations between large- and active-scale modes. We have tested this by letting the modes at wavelet levels 0, 1 and 2 each be driven independently by the stochastic process (7), the remaining levels undergoing KS dynamics; the resulting evolution is visually and statistically remarkably close to that of the full KS equation [20]. That is, purely stochastic large-scale evolutions appear to have the same effect as their deterministically derived counterparts in the way they drive chaotic dynamics at the active scales: the dynamical contributions of the large scales in the KS equation are essentially random. As a consequence, in a short model for the spatiotemporally complex dynamics, it is sufficient to use the simple linear random process (7) to simulate the effect of the noisy large scales which are present in a long system, thereby providing the 'heat bath' which keeps the system 'alive' and away from a simple equilibrium.

An interesting test of robustness, relevant to our modeling, is the extent of variation in the large-scale driving tolerated by the dynamics. It turns out that variations in the *rate* of large-scale forcing have little effect on the active-scale dynamics, which compensate for excessively rapid or slow forcing and respond at their intrinsic time scales. This is unsurprising if indeed, as is suggested by other experiments reported above, the sole purpose of the large scales is to provide Gaussian excitation, for then altering large-scale time scales merely varies the rate at which the Gaussian distribution is sampled.

On the other hand, the dynamics are sensitive to the driving *amplitudes*: excessive energy at the large scales induces rapidly traveling structures and shock-like features. Such behavior may be interpreted, at least qualitatively, by the observation that from the perspective of the active levels, high large-scale energy has the effect of changing the local mean, which by the Galilean invariance of the KS equation (2) is equivalent to imposing a drift. The traveling and shock solutions are also reminiscent of those observed in a destabilized version of the KS equation [21], in which the linear dispersion relation is shifted up uniformly through an additional $(\varepsilon^2 - 1)u$ term, $\varepsilon > 1$, on the right-hand side of (2). For the purposes of modeling, it is thus necessary to take more care in simulating the amplitudes than the time scales of the neglected modes.

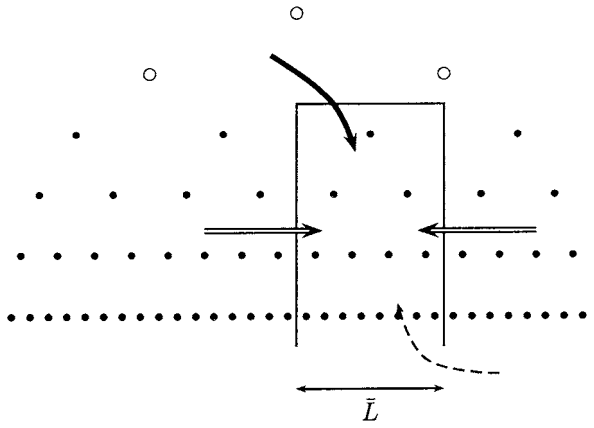

Figure 5. Simplified 'cartoon' representation of our approach to extracting externally forced models for a spatially localized subsystem of the full system, as in Section 3.1.

3. Spatially Localized Models

We now combine the above ingredients into the construction of localized models for spatiotemporally chaotic dynamics. We have shown that the dynamics are localized in space and strongly scale-dependent, and that the well-localized wavelet modes enable a good characterization of the KS dynamics and a detailed understanding of the relevant contributions of respective wavelet levels. As previously discussed, we wish to critically examine the idea of a large, extensively chaotic system in the 'thermodynamic limit' being composed of smaller, weakly interacting subsystems of relatively low dimension, by the explicit construction of such candidate spatially localized subsystems. This motivates us to extract a 'box' of internal wavelet modes $\{a_\alpha\}$ evolving according to (8), using the results on the scale-by-scale structure to choose appropriate external forcing $\{b_{\alpha'}\}$.

As depicted schematically in Figure 5, for our localized model we extract a subset **B** of the full wavelet hierarchy, of wavelets centered on a domain of length $\bar{L} = 2^{-j_0}L$; typically we use $j_0 = 2$ for a full $L = 100$ system, to yield short systems of length $\bar{L} = 25$. With this choice of lengths, we may exploit the results of the previous sections and of [22] on the separation of scales and contribution of different wavelet levels to the $L = 100$ KS dynamics, which carry over to multiples of L by powers of two. We choose these parameters for various reasons:

- We know that $\bar{l}_c \approx 25$ is a good estimate for a characteristic dynamic interaction length, so $\bar{L} = 25$ seems a reasonable length for a localized model.
- Larger $\bar{L}$ implies more complex internal dynamics, and requires a higher-dimensional model; for large enough $\bar{L}$, no external forcing is needed to obtain spatiotemporally complex dynamics, rendering the modeling redundant. In contrast, for the range $\bar{L} \in [20, 30]$, various types of 'simple' attractors exist for the KS equation, including fixed points, standing and traveling waves and heteroclinic cycles [11].
- For given $\bar{L}$, a larger 'full system' length L just adds more large-scale levels, providing slow Gaussian forcing, and contains additional boxes which do not significantly interact with the subsystem we are interested in, being separated from it by a distance greater than $\bar{l}_c$.

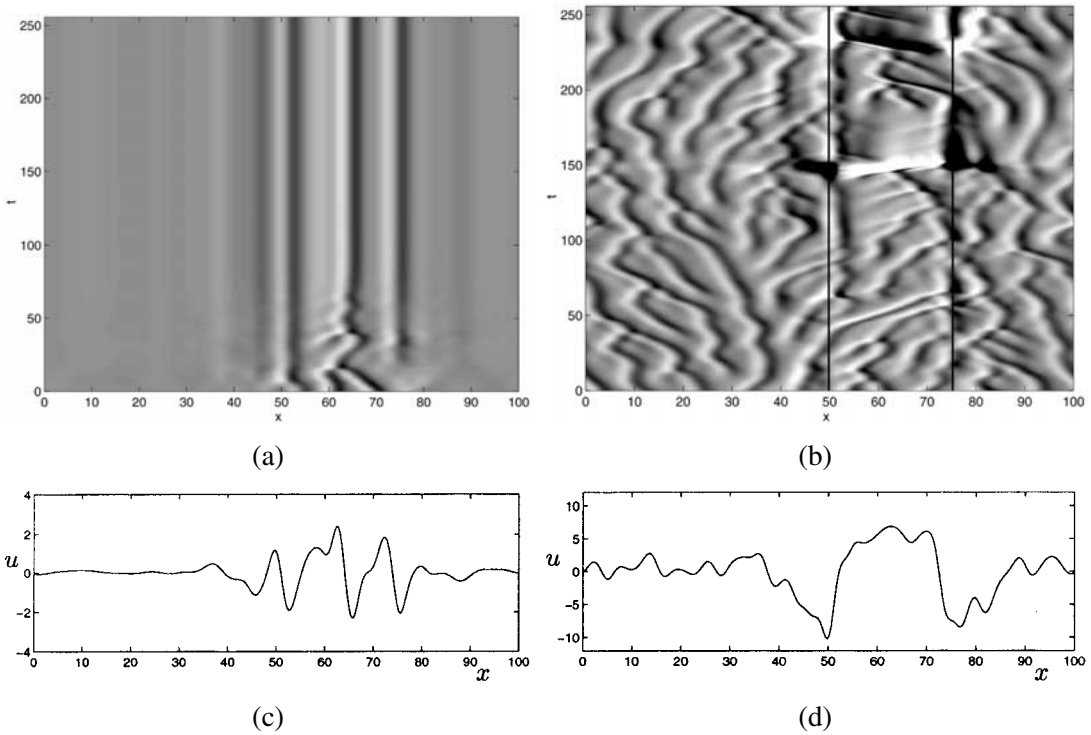

Figure 6. Local, nonperiodized model for the modes in the box of Figure 5. (a) No external forcing implies rigid dynamics; the $t = 150$ cross-section is shown in (c). (b) Forcing at external modes at levels $j = 0$–5 leads to excessive amplitudes and boundary effects, as in the $t = 150$ cross-section shown in (d).

3.1. Localized, Nonperiodic Models with Forcing

In the full KS equation, each local 'box' of wavelet modes interacts with its neighbors and with the large scales, which act as external forcing; and, provided the system size is sufficiently large, the dynamics are locally unaware of the global periodicity, the bulk dynamics being independent of boundary conditions. Thus it may seem reasonable to seek models in which the local box is forced from the large scales and external adjacent modes, without imposing the constraint of periodicity, as schematically portrayed in Figure 5. One would expect that success would depend on feeding in the 'correct' statistics for the active scale external modes, as described above [22]. It turns out, however, that in such models, the translational symmetry of the KS dynamics is broken too drastically, leading to atypical dynamics, as previously observed in preliminary unpublished experiments of J. Elezgaray (referred to in [14]).

In these experiments, the modes $\{a_\alpha\}$ inside the chosen 'box' are evolving within the localized, forced model, being driven by the outside modes $\{b_{\alpha'}\}$ according to (8). Our experimental procedure is described in Section 2.4, and in more detail in [20]; in summary, we integrate a full KS equation for the complete hierarchy of wavelet modes, and at each time step, all the modes outside the short box are either set to zero, or overwritten by values obtained from an independent full KS integration running simultaneously.

Figure 6 shows some representative results. In Figure 6a, the modes inside the box, rooted at wavelet level 2, evolve in the absence of any forcing: $b_{\alpha'} = 0, \alpha' \notin \mathbf{B}$. Such a system rapidly settles down to a steady state, with fixed peaks, as seen in the $t = 150$ cross-section in (c). In

the absence of both forcing and periodic boundary conditions, therefore, this 15-dimensional dynamical system (containing wavelet levels $j = 2$–5) remains rigid.

The opposite extreme is shown in Figure 6b, in which the box **B** is driven at all large- and active-scale external modes $\alpha' \notin \mathbf{B}$ with time series $b_{\alpha'}(t)$ obtained from a full independent KS integration (5). The forcing terms thus automatically have the 'correct' statistics at the different levels (note that the figure is reconstructed on $L = 100$ from both the internal modes of the model and the forcing terms). The large amplitudes (particularly at the boundaries of the box) and rapid fronts apparent in Figure 6b, and in the $t = 150$ cross-section in (d), are due to the disruption of the normal feedback mechanisms, so that wavelet coefficients may grow abnormally before they decay. Specifically, the evolution (5) of the external modes $b_{\alpha'}$, which provide the driving time series, is independent of the modes a_α within the box, so that they cannot provide the 'correct' compensation for growth in the internal modes, sometimes serving rather to reinforce unusually large amplitudes (relative to those observed in a full KS run such as that of Figure 1).

The origin of the difficulties may be traced to the fact that the set **B** of modes internal to the model includes ones that are (sufficiently) linearly unstable and autonomously excited, instead of being slaved to the forcing. Consider the evolution of the differences $d_\alpha = a_\alpha - b_\alpha$ between internal modes a_α evolving according to (8), and corresponding driving coefficients b_α satisfying (5): the d_α obey the equation

$$\dot{d}_\alpha = \sum_{\alpha' \in \mathbf{B}} l_{\alpha\alpha'} d_{\alpha'} + \sum_{\alpha', \alpha'' \in \mathbf{B}} n_{\alpha\alpha'\alpha''}(d_{\alpha'} b_{\alpha''} + d_{\alpha''} b_{\alpha'} + d_{\alpha'} d_{\alpha''}) + \sum_{\alpha' \in \mathbf{B},\ \alpha'' \notin \mathbf{B}} (n_{\alpha\alpha'\alpha''} + n_{\alpha\alpha''\alpha'}) d_{\alpha'} b_{\alpha''}, \tag{9}$$

which may be rewritten as

$$\dot{d}_\alpha = \sum_{\alpha' \in \mathbf{B}} [l_{\alpha\alpha'} + g_{\alpha\alpha'}(t)] d_{\alpha'} - \tfrac{1}{2} \sum_{\alpha', \alpha'' \in \mathbf{B}} n_{\alpha'\alpha''\alpha} d_{\alpha'} d_{\alpha''}. \tag{10}$$

Here we have used the identity $n_{\alpha'\alpha''\alpha} = -n_{\alpha\alpha'\alpha''} - n_{\alpha\alpha''\alpha'}$ [14], and defined the parametric driving term $g_{\alpha\alpha'}(t) = -\sum_{\alpha''} n_{\alpha'\alpha''\alpha} b_{\alpha''}(t)$, which has vanishing mean since all the $b_{\alpha''}$ have zero time average (see Figure 3).

If only a single internal mode α is driven by all others, then the nonlinear term in (10) vanishes (since $n_{\alpha\alpha\alpha} = 0$) and the difference d_α grows or decays exponentially, on average, depending on the sign of $l_{\alpha\alpha}$, that is, according to the linear stability or instability of mode α. That is, a model in which a single large-scale mode is driven by all others, will blow up, while a small-scale (high-j) mode will be synchronized to the control run.

In the general case in which **B** contains more than one element, the nonlinear term in (10) conserves energy, but transfers it among the internal modes, and the situation is more complicated; stability and instability depend on the operator $A_{\alpha\alpha'}(t) = l_{\alpha\alpha'} + g_{\alpha\alpha'}(t)$. However, we expect that if the internal modes are (sufficiently) linearly unstable, with all the stable modes participating in the driving, then $A_{\alpha\alpha'}(t)$ is, on average, positive definite, and the model energy grows exponentially. Conversely, if all large-scale modes are involved in the driving, and the internal modes $\alpha \in \mathbf{B}$ are all linearly stable, then $l_{\alpha\alpha'}$ (and thus, on average, $A_{\alpha\alpha'}(t)$) is negative definite, the difference decays, and tracking to the control run occurs: sufficiently many low modes uniquely determine the asymptotic dynamics, as small scales are slaved to large scales – in fact this can be shown rigorously under slightly stronger conditions [20].

More generally, if the 'box' contains some linearly unstable and some stable modes, then energy transfer from large to small scales prevents blow-up of the model. However, the possibility of tracking, that is, $d_\alpha \to 0$ for $\alpha \in \mathbf{B}$, depends on the linear part of (10), that is, on $A_{\alpha\alpha'}(t)$. We expect, from (10), that the presence of (sufficiently) unstable modes among the set $\mathbf{B}$ of internal modes implies positive eigenvalues of $A_{\alpha\alpha'}(t)$, and hence, instability of the synchronized state $\{d_\alpha = 0\}$. Our experience is that (for $L = 100$) any modes at wavelet levels $j \leq 3$ satisfy the requirements for instability; the situation for $j = 4$ is less clear. Thus, in models of the form of Figure 5, the modes $a_\alpha, \alpha \in \mathbf{B}$ in the box fail to synchronize to the behavior of the corresponding modes b_α satisfying the full KS equation. For more discussion, and results of numerical experiments confirming all the above scenarios, see [20, secs. 5.3, 6.1].

These results and simulations such as that of Figure 6b pose a serious problem for the construction of non-periodized, externally forced local models: since undesirable results including excessive amplitudes occur even if the forcing is from a full KS integration – that is, the driving necessarily has all the 'correct' statistical properties – we can hardly expect better results from more simplified types of external random fluctuation. The problem of excessive growth seems destined to occur whenever our model is able to support its own dynamics by containing unstable modes. Consequently, these conclusions do not necessarily depend on our wavelet formulation, or even on the KS equation; they may apply more generally to driving and synchronization of a localized model through boundary forcing.

Numerous other experiments including various types of external forcing – for instance, forcing only at certain wavelet levels, or only from a 'halo' of nearest neighboring active-scale modes – essentially confirm the above observations. We find in general that for models of the type depicted in Figure 5, one of two possibilities occurs, broadly corresponding to the two extreme cases of Figures 6a and 6b:

- The first case occurs when the excitation of the internal modes is weak; for instance, when it arises from the large scales, or is due only to a few external modes, as in Figure 7a, in which the modes in the box are forced only at level $j = 3$. In this case, the model dynamics are rigid; there may be a fluctuating peak in the interior, undergoing some typical 'events', but peaks at the boundaries of the model are stationary and excessively constrain the internal dynamics.
- In the second scenario, the internal modes are influenced more strongly by exterior modes, usually when forcing is at the active-scale levels $j = 4$ and/or 5, such as in Figure 7b. In this situation, more realistic dynamics can occur, including motion of the peaks; but there are mismatches at the boundaries and large-scale internal modes tend to be excited excessively due to failure of the standard damping mechanisms, leading to large amplitudes, high local means and rapid fronts.

In some experiments, the conditions for both these anomalies are satisfied, leading to even more disrupted model dynamics. The effect of breaking the translational symmetry, so that the modes at the edges of the box are essentially inequivalent to those in the center, is too drastic, and such local models, it appears, cannot reproduce the spatiotemporally complex dynamics typically observed in the KS equation. Another difficulty with such externally forced models is that, while they may be readily investigated numerically, they appear too complicated to be analytically tractable.

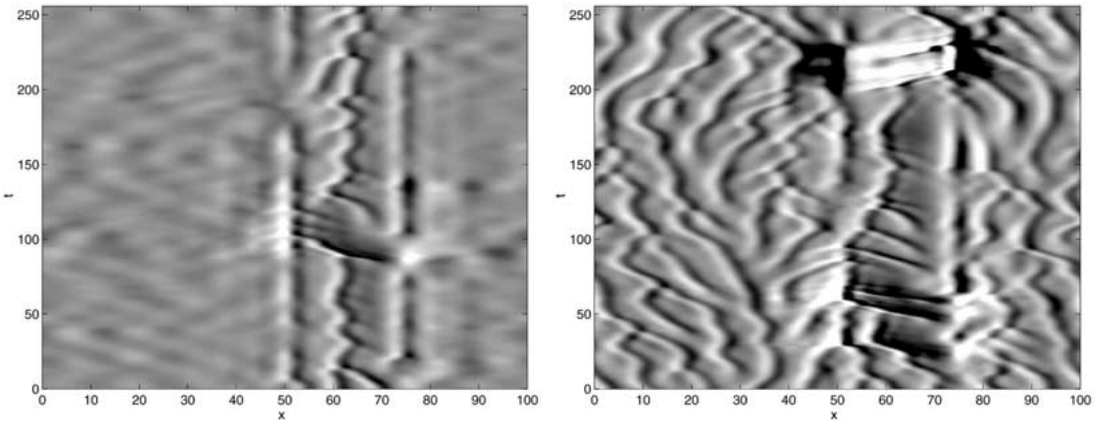

Figure 7. Nonperiodized model, with modes in the distinguished box forced from the active scales of an independent control run at (a) level $j = 3$, (b) levels $j = 4$ and 5.

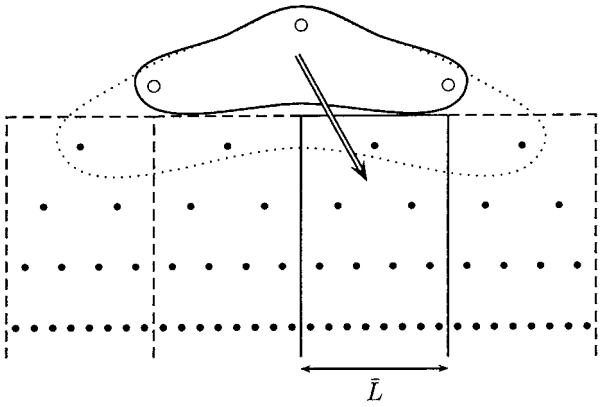

Figure 8. Schematic representation of periodized models of a short subsystem, forced from the largest-scale external and/or internal modes, as in Sections 3.2 and 3.3.

3.2. Periodized Models with Aperiodic Forcing

In the light of the above-mentioned difficulties, we have investigated another class of models, in which active-scale interactions are restored by periodizing. A motivation for imposing periodic boundary conditions is to replace the influence of missing adjacent 'external' modes by distant 'internal' modes [3], with the advantage of eliminating the drastic inequivalence between internal modes at the center and boundaries of the model, and thereby better approximating the infinitesimal translation symmetry of the KS equation (Fourier-based models of short periodic systems, which preserve the translation invariance, have been studied in [5]).

As before, we include a caricature of this approach in Figure 8. In practice, numerical experiments with such models are performed by selecting a 'distinguished box' of length $\bar{L} = 2^{-j_0} L$, and at each time step, setting wavelet coefficients in all adjacent boxes to the corresponding values in the distinguished box (where the centers of 'corresponding' wavelets are separated by a multiple of $\bar{L}$). That is, essentially we only evolve the modes within the distinguished box, subject to large-scale forcing from wavelet levels $j < j_0$.

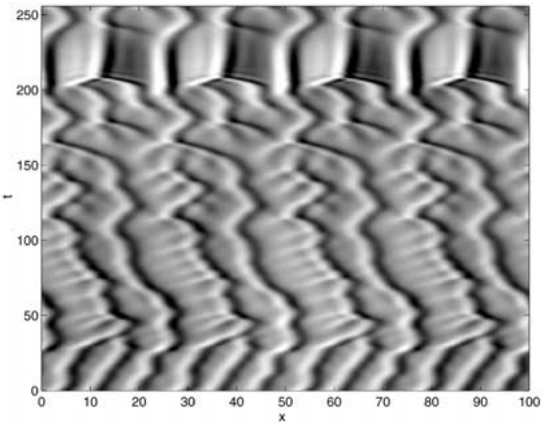

Figure 9. Periodized model, forced by levels $j = 0$ and 1 of an independent KS integration.

The theoretical basis and a consistent notation and formalism for such models, analogous to (8), are introduced in chapter 3 of [20], which also includes the straightforward demonstration that, in the absence of any large-scale forcing at $j < j_0$, a length L system periodized from level j_0 is exactly equivalent to an $\bar{L}$-periodic KS equation. In particular, for $L = 100$, $\bar{L} = 25$, without the largest wavelet levels the periodized model rapidly converges to a trimodal cellular state, known to be the attractor for $\bar{L} = 25$ [11]. If we retain levels $j < j_0$, however, such models provide a systematic approach to interpreting a smaller periodic system as a subsystem of a larger one, by retaining an influence of large scales as driving inputs to short periodic boxes.

We may also write evolution equations for the internal modes in the box, interpreting them as wavelet coefficients for a basis periodized on a domain of length $\bar{L}$. However, the Galerkin evolution equations are not particularly tractable, containing $2^{j_0} - 1$ forcing terms in the equation for each mode. Furthermore, the large-scale forcing term is not $\bar{L}$-periodic, and hence acts differently on the different boxes, as is apparent from the representation of Figure 8. Consequently, an initially $\bar{L}$-periodic system will not remain periodic, unless constrained to be so. This is achieved in our simulations by choosing a distinguished box *a priori*, and after each time step overwriting the coefficients in the other boxes by those in the distinguished box, as described above.

A typical experiment of this kind is shown in Figure 9, in which we force from levels $j = 0$ and 1. We note that the large-scale driving (which is essentially equivalent to Gaussian noise) maintains the periodized subsystem away from the steady state; and that local 'events' reminiscent of those in STC, such as traveling structures and creation and collision of peaks, occur persistently. That is, the large-scale forcing keeps the system 'alive'. However, visual inspection indicates that the dynamics of this system are rather unusual, a conclusion supported by comparison of long-time statistical calculations of the model power spectrum and distributions at different wavelet levels with Figures 2 and 3. The inconsistencies may be related to occasional anomalous large-amplitude shock-like events, observed for instance near $t = 225$ of Figure 9, which are associated with excessive energy at the largest internal scales of the model, similar to those previously seen when forcing excessively at the large scales.

While localized periodic models with aperiodic large-scale forcing may seem natural to capture the effect of the large-scale modes on the active scales, and do appear to reproduce some of the typical KS events, the presence of atypical structures and shocks due to the

asymmetry of the forcing term indicates that this type of model is inadequate. $\bar{L}$-periodic forcing leads to a more tractable model, and we now turn to this.

3.3. Periodized Models with Periodic Forcing

We avoid the problems due to aperiodicity, described in Sections 3.1 and 3.2, by averaging the large-scale forcing terms in space, to render them $\bar{L}$-periodic. In practice, this is equivalent to averaging corresponding wavelet coefficients over the boxes, after performing a time step with aperiodic driving; and this latter method is the one we have used for our numerical experiments.

Since all wavelets and driving terms in this model are now $\bar{L}$-periodic, it is possible to write an effective PDE for the solution inside a box such as one of those in Figure 8; the existence of such a relatively simple formulation is a major reason for preferring such periodized models. By writing out explicitly the wavelet Galerkin formulation of the KS equation, considering the evolution of modes within the box subject to periodicity and large-scale periodic forcing, and then 'inverting' the Galerkin procedure, one finds that the solution $\bar{u}(x, t)$ on the box satisfies a KS equation with external forcing (compare (3)),

$$\bar{u}_t = \mathcal{L}\bar{u} + \bar{u}\mathcal{D}\bar{u} + \mathcal{D}(\bar{u}\bar{v}) + \mathcal{L}\bar{v} + \bar{w}, \tag{11}$$

with $\bar{L}$-periodic boundary conditions [20, sec. 3.3]. Here it turns out that $\bar{v} = 0$, since it is the projection of the large-scale modes $j < j_0$ onto the scales $j \geq j_0$: the periodization removes linear and parametric influences of large scales. Similarly, $\bar{w}$ is the projection of the nonlinear term reconstructed from the large scales, onto the small scales. This does not vanish in general (since the subspaces in a multiresolution analysis are not closed under multiplication and differentiation), but there are some special cancellations for symmetric wavelets. This procedure thus yields an effective PDE for a short system, subject to weak averaged forcing $\bar{w}$ from the large scales:

$$\bar{u}_t = \mathcal{L}\bar{u} + \bar{u}\mathcal{D}\bar{u} + \bar{w}. \tag{12}$$

We have performed experiments for $L = 100$ ($\bar{L} = 25$) with such forcing, in which the driving from levels $j = 0$ and 1 is derived from an independent KS integration (see Figure 10a). The atypical dynamics and excessive amplitudes which were prevalent in the aperiodic models have disappeared under periodization, but the large-scale forcing $\bar{w}$, while nonzero, appears too weak under the averaging to sustain complex spatiotemporal activity. In related experiments with sinusoidal or other forcing at the large scales, the system also settled down to a steady cellular state.

The formulation (12) for a short local system modeling a subsystem of a larger spatiotemporally complex system, while showing promise for analytical investigation, appears to be unsuccessful in numerical experiments, at least for the parameter values we have investigated; the periodization seems to eliminate too much of the desirable driving. However, we can use the ideas leading to (11) and (12) to suggest extensions of the model, in which the forcing is periodic and thus does not incur the undesirable effects of symmetry-breaking, but there is still a strong direct influence on the active scale modes. One possibility is to introduce a nonzero function $\bar{v}$ into (11), to simulate the effects of parametric and linear large-scale driving; this may be a promising avenue for future exploration. An alternative, which we explore briefly here, is to simulate the driving effect of the large Gaussian scales on the box, much of which is lost by periodization, by *explicitly driving* the largest-scale internal modes.

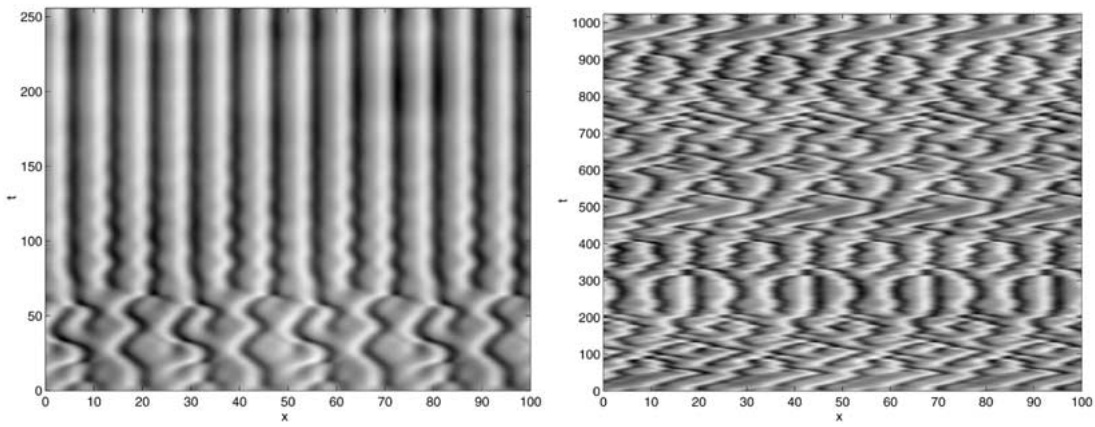

(a) (b)

Figure 10. Periodized model with periodized forcing from an independent KS integration, driving at (a) levels $j = 0$ and 1; (b) levels $j = 0$ and 1, and forcing the lowest internal mode at $j = 2$.

Figure 10b shows the result of an experiment with $\bar{L}$-periodic forcing in which, in addition to driving at levels $j = 0$ and 1 via the averaged $\bar{w}$, the lowest internal mode at $j = 2$ is also driven from an independent KS integration. The dynamics over most of the time interval shown (apart from those times at which the level 2 forcing is unusually small) look remarkably like those of the full KS equation; this is confirmed by long-time statistical calculations of spectra and PDFs. By comparison with Figure 10a, it is apparent that the $j = 2$ excitation has by far the strongest effect, the periodized forcing from levels 0 and 1 exerting little influence on the complex dynamics. It is thus reasonable to ask whether the external forcing $\bar{w}$ from $j = 0$ and 1 is necessary at all; what happens if we just drive at level 2? Simulations confirm that, unsurprisingly, driving the periodized model at level $j = 2$ with a time series taken from the control run is sufficient to maintain complex dynamics and good statistics. *Forcing at only the lowest internal mode of a periodized subsystem captures the effect of the large scales on the short local model.*

3.4. Short Models with Spatiotemporally Complex Dynamics

It is now readily apparent that this short periodized model, in the absence of the large-scale term $\bar{w}$, is exactly a full KS equation (2) on a short $\bar{L}$-periodic domain, in which the lowest level is externally specified. This motivates us to propose an autonomous 'minimal model': small L-periodic KS systems with forcing (where we now use L rather than $\bar{L}$ to emphasize that these are not necessarily subsystems of larger systems). Within this framework, a wide range of experiments is possible, encompassing driving with different amplitudes, time scales and temporal characteristics, as well as variations in the length of the domain (implying differing elementary attractors in the absence of forcing). In the present study, we present the results of only a few such simulations, to demonstrate that such short systems with forcing form a reasonable model for STC in the KS equation.

Our construction of the minimal model for a short box, driven at its largest scale, is confirmed by some of our previous conclusions:

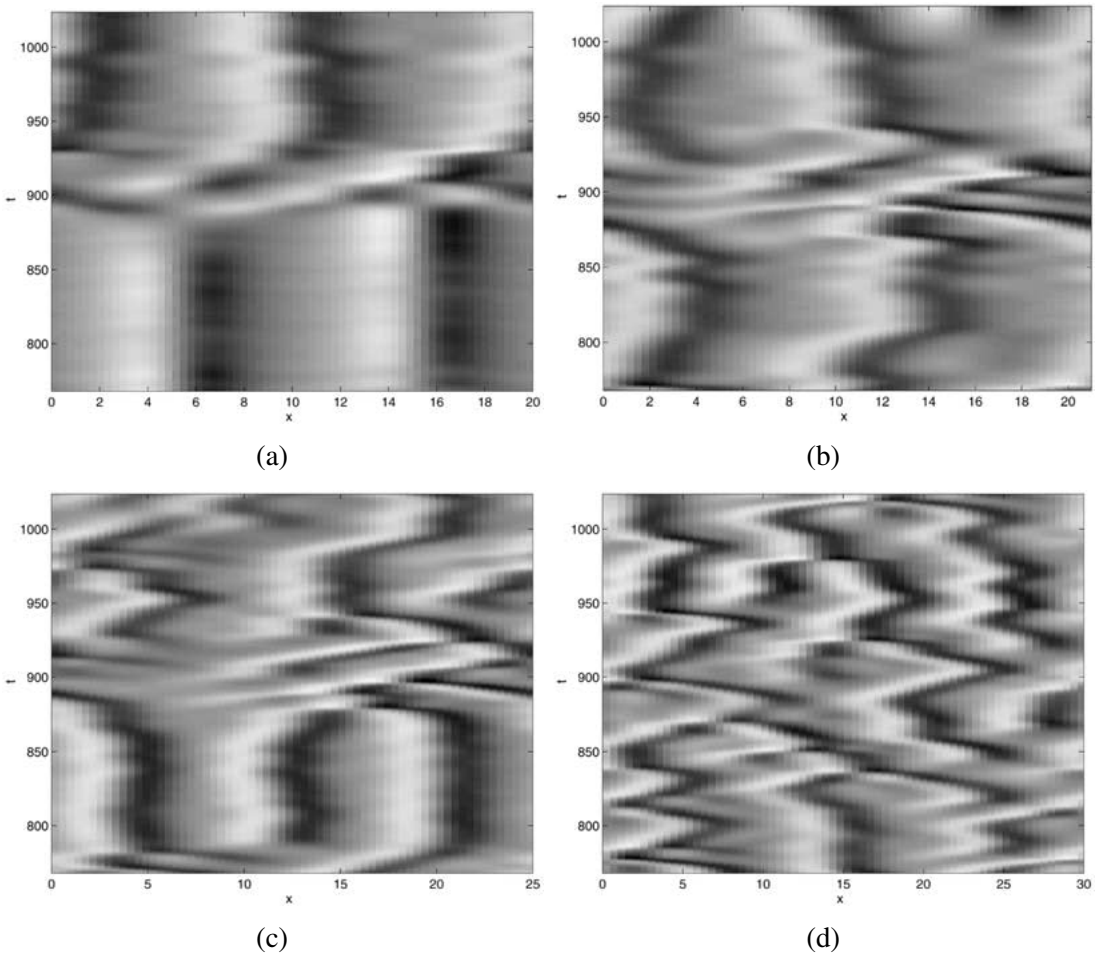

Figure 11. Short systems for a range of L, randomly driven at their lowest wavelet level by a suitably chosen colored Gaussian process: (a) $L = 20$, (b) $L = 21$, (c) $L = 25$, (d) $L = 30$.

- Within the STC regime, the dynamics are spatially localized, but interactions up to a length $l \sim \bar{l}_c \approx 25$ are dynamically relevant.
- The typical interactions of coherent structures occur at the active scale levels, but the large scales provide the excitation essential to sustain the complex spatiotemporal dynamics.
- The strength of the large-scale driving plays an important role; forcing that is too weak may lead to collapse into a cellular state, while unduly powerful driving leads to large amplitudes and rapidly traveling peaks, or even to a shock-like solution.
- The temporal structure and correlation time of the driving has a relatively small influence.
- To avoid excessive growth, the forcing should be spatially L-periodic; but it should be sufficiently strong at the largest scales within the model to drive the characteristic spatiotemporal behavior.

We have performed numerical simulations on short boxes of a range of lengths, in which the excitation of the largest-scale internal mode is derived from the autonomous stochastic

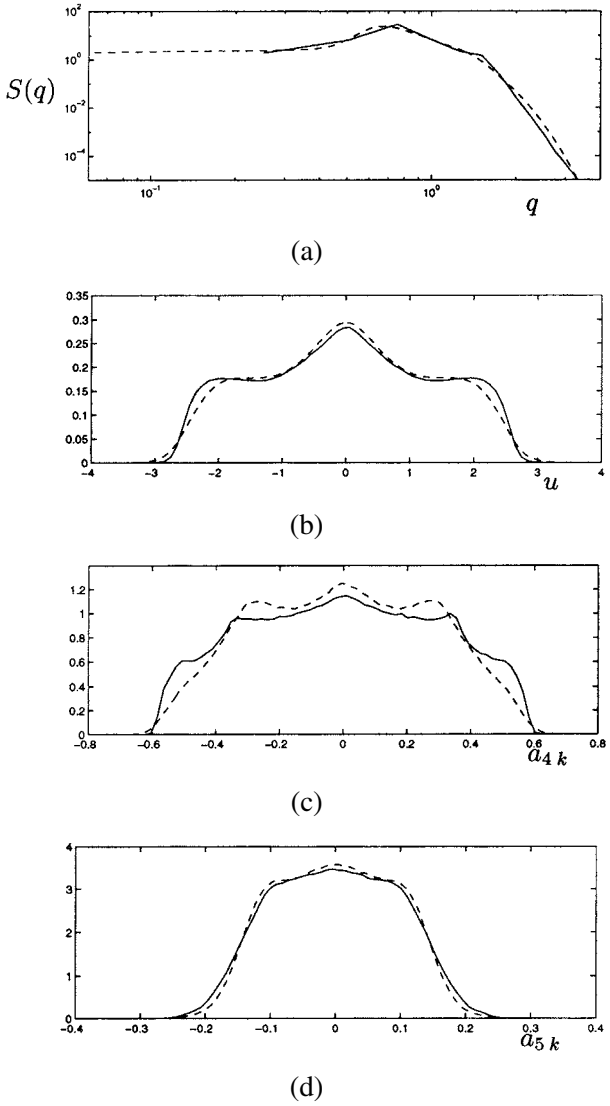

Figure 12. Comparison of statistics for $L = 25$ model driven by colored Gaussian noise at the lowest wavelet level (solid lines), with statistics of full KS equation on $L = 100$ (dashed lines): (a) power spectra (see Figure 2); (b) PDF of pointwise values of the field u; (c) PDF of wavelet level $j = 2$ of model, compared with $j = 4$ for the $L = 100$ full system; and (d) model $j = 3$ PDF, compared with full $j = 5$ PDF (compare Figure 3).

process (7) (Langevin equation with colored noise); as described previously, this form is motivated by the effective forced Burgers equation description of the large-scale dynamics and the fact that this colored Gaussian noise model effectively simulates the statistics and dynamical effects of the large scales.

Figure 11 shows some representative results. It appears from (a) for $L = 20$ that if L is too short, the system is too highly constrained to generate the typical events necessary for STC, and settles into an apparent heteroclinic cycle; this is consistent with the existence of a characteristic dynamical interaction length $\bar{l}_c$. However, the systems with $L \geq 21$ all

display sustained chaotic behavior closely reminiscent of the STC state for long KS systems, as borne out by a comparison of the statistics between the $L = 25$ model of Figure 11c and the full KS equation of Figure 1, some of which are shown in Figure 12. Note however that by comparison with the full system, the PDFs of u in (b), and of the level 2 wavelets in (c), display a trend towards a cellular state, evidenced by broader distributions, with the model spending more time at large amplitudes; this effect is readily understood by recalling that an unforced $L = 25$ system tends to the attracting cellular state, so that the driven model will temporarily approach such a state over time intervals during which the stochastic forcing has small amplitude.

It is interesting to note that similar results are obtained if the autonomous forcing at the lowest wavelet level is chosen to be deterministic, sinusoidal in time: the qualitative dynamics resemble those typical for STC in a large KS system almost as often, for a range of L, as in the case of random forcing; and (because the sinusoidal driving does not linger near zero for extended intervals) some of the statistics appear to be even closer to those of the full system than those shown in Figures 12b and 12c. This suggests that the Gaussian statistics at the large scales, and the temporal characteristics of the colored noise process, are inessential to drive active-scale chaotic dynamics. Thus it seems that both deterministic and stochastic forcing at the lowest wavelet level of a short KS system are capable of driving the system sufficiently that it generates complex dynamics similar to those observed in the large-L thermodynamic limit. Such a relatively low-dimensional model of a short system with large scales forced with externally generated processes appears to qualify as a 'minimal box' containing the ingredients for STC in the KS equation, and we are continuing to study such systems to explore the origins and nature of spatiotemporal chaos.

4. Conclusion

The wavelet decomposition has given us insight into the localization of KS dynamics in space and scale. Motivated by these results, we have proposed and investigated various wavelet-based models for short, forced subsystems of an extended spatiotemporally complex system. A major conclusion is that the relevant symmetries, implied by periodic boundary conditions, are essential both in the system and in the forcing, to avoid excessive amplitudes and atypical events. Within the context of periodized subsystems with periodic forcing, driven also at the largest-scale internal modes, we have discovered model systems that appear to emulate the STC of the full KS equation.

We deduce that short, driven systems, provided they have length at least of order of the dynamical interaction length, can sustain spatiotemporal complexity. In this view, the attractor for the appropriately forced short systems is in some sense similar to that in the extensive limit. We postulate an, as yet purely heuristic, description for this idea that the large system may be fully understood in terms of the dynamics of smaller subsystems, by writing

$$\text{`}\mathcal{A}_L \approx \oplus \mathcal{A}_{\tilde{L}}\text{'},$$

where $\mathcal{A}_L$ represents the attractor for a length L system; of course, this representation presupposes the, as yet unproven, extensivity of the KS equation. This picture deduced from our experiments of Section 3.4 allows us to speculate that the main difference between 'large' and 'small' systems is the noisy dynamics at the lowest modes which drive the typical events. This noise arises due to the collective interactions of the subsystems; and the threshold to sustained

STC occurs when sufficiently many subsystems interact to maintain the Gaussian large-scale dynamics, which in turn feed into the subsystems and maintain activity within them, in a similar way to our latest experiments.

Acknowledgements

RW would like to thank J. Elezgaray for providing his computer code for some of the wavelet transform calculations. This work was partially supported by DoE grant DE-FG02-95ER25238 and by a Charlotte Elizabeth Procter Fellowship at Princeton University.

References

1. Aubry, N., Holmes, P., Lumley, J. L., and Stone, E., 'The dynamics of coherent structures in the wall region of a turbulent boundary layer', *Journal of Fluid Mechanics* **192**, 1988, 115–173.
2. Barabási, A.-L. and Stanley, H. E., *Fractal Concepts in Surface Growth*, Cambridge University Press, Cambridge, 1995.
3. Berkooz, G., Elezgaray, J., and Holmes, P., 'Coherent structures in random media and wavelets', *Physica D* **61**, 1992, 47–58.
4. Browning, G. L., Henshaw, W. D., and Kreiss, H.-O., 'A numerical investigation of the interaction between the large and small scales of the two-dimensional incompressible Navier–Stokes equations', preprint, April 1998; UCLA CAM Report 98-23, 1998.
5. Dankowicz, H., Holmes, P., Berkooz, G., and Elezgaray, J., 'Local models of spatio-temporally complex fields', *Physica D* **90**, 1996, 387–407.
6. Elezgaray, J., Berkooz, G., and Holmes, P., 'Wavelet analysis of the motion of coherent structures', in *Progress in Wavelet Analysis and Applications*, Y. Meyer and S. Roques (eds.), Editions Frontières, Gif-sur-Yvette, 1993, pp. 471–476.
7. Elezgaray, J., Berkooz, G., and Holmes, P., 'Large-scale statistics of the Kuramoto-Sivashinsky equation: A wavelet-based approach', *Physical Review E* **54**, 1996, 224–230.
8. Halpin-Healy, T. and Zhang, Y.-C., 'Kinetic roughening phenomena, stochastic growth, directed polymers and all that', *Physics Reports* **254**, 1995, 215–414.
9. Hayot, F., Jayaprakash, C., and Josserand, C., 'Long-wavelength properties of the Kuramoto–Sivashinsky equation', *Physical Review E* **47**, 1993, 911–915.
10. Holmes, P., Lumley, J. L., and Berkooz, G., *Turbulence, Coherent Structures, Dynamical Systems and Symmetry*, Cambridge University Press, Cambridge, 1996.
11. Hyman, J. M., Nicolaenko, B., and Zaleski, S., 'Order and complexity in the Kuramoto–Sivashinsky model of weakly turbulent interfaces', *Physica D* **23**, 1986, 265–292.
12. Kardar, M., Parisi, G., and Zhang, Y.-C., 'Dynamic scaling of growing interfaces', *Physical Review Letters* **56**, 1986, 889–892.
13. L'vov, V. S., Lebedev, V. V., Paton, M., and Procaccia, I., 'Proof of scale invariant solutions in the Kardar-Parisi-Zhang and Kuramoto–Sivashinsky equations in 1+1 dimensions: Analytical and numerical results', *Nonlinearity* **6**, 1993, 25–47.
14. Myers, M., Holmes, P., Elezgaray, J., and Berkooz, G., 'Wavelet projections of the Kuramoto–Sivashinsky equation I. Heteroclinic cycles and modulated traveling waves for short systems', *Physica D* **86**, 1995, 396–427.
15. Perrier, V. and Basdevant, C., 'Periodical wavelet analysis, a tool for inhomogeneous field investigation. Theory and algorithms', *La Recherche Aérospatiale* **1989**(3), 1989, 53–67.
16. Pomeau, Y., Pumir, A., and Pelce, P., 'Intrinsic stochasticity with many degrees of freedom', *Journal of Statistical Physics* **37**, 1984, 39–49.
17. Pumir, A., 'Statistical properties of an equation describing fluid interfaces', *Journal de Physique* **46**, 1985, 511–522.
18. Sneppen, K., Krug, J., Jensen, M., Jayaprakash, C., and Bohr, T., 'Dynamic scaling and crossover analysis for the Kuramoto–Sivashinsky equation', *Physical Review A* **46**, 1992, R7351–R7354.

19. Toh, S., 'Statistical model with localized structures describing the spatio-temporal chaos of Kuramoto–Sivashinsky equation', *Journal of the Physical Society of Japan* **56**, 1987, 949–962.
20. Wittenberg, R. W., 'Local dynamics and spatiotemporal chaos. The Kuramoto–Sivashinsky equation: A case study', Ph.D. Thesis, Princeton University, 1998.
21. Wittenberg, R. W., 'Dissipativity, analyticity and shocks in the (de)stabilized Kuramoto–Sivashinsky equation', 2000, in preparation.
22. Wittenberg, R. W. and Holmes, P., 'Scale and space localization in the Kuramoto–Sivashinsky equation', *Chaos* **9**, 1999, 452–465.
23. Yakhot, V., 'Large-scale properties of unstable systems governed by the Kuramoto–Sivashinski equation', *Physical Review A* **24**, 1981, 642–644.
24. Zaleski, S., 'A stochastic model for the large scale dynamics of some fluctuating interfaces', *Physica D* **34**, 1989, 427–438.